Density dependence of the dynamical processes governing the velocity autocorrelation function of a quantum fluid

Eleonora Guarini,[1,*] Martin Neumann,[2] Stefano Bellissima,[3] Daniele Colognesi,[3] and Ubaldo Bafile[3]

[1]*Dipartimento di Fisica e Astronomia, Università degli Studi di Firenze, via G. Sansone 1, I-50019 Sesto Fiorentino, Italy*

[2]*Fakultät für Physik der Universität Wien, Strudlhofgasse 4, A-1090 Vienna, Austria*

[3]*Consiglio Nazionale delle Ricerche, Istituto di Fisica Applicata "Nello Carrara", via Madonna del Piano 10, I-50019 Sesto Fiorentino, Italy*

(Received 23 September 2019; published 9 December 2019)

We present an exponential mode analysis of the dynamical processes determining the time behavior of the Kubo velocity autocorrelation function (KVAF) of fluid para-H_2, as obtained by ring polymer molecular dynamics simulations at various fluid densities. The mechanisms contributing to the decay of the KVAF are thoroughly characterized at a slightly supercritical temperature, in a density interval ranging from the critical point to the fluid-solid transition. We show that the quantum nature of the system does not influence the specific phenomena and decay channels through which a loss in velocity correlation takes place, since these are the same as found in classical fluids. Similarly, a dynamical crossover is observed with increasing density, signaling the onset of a transverse-like dynamics like in classical systems. We also investigate the effect of density on the processes contributing to the most relevant property of a quantum fluid, namely, the large values of the total and zero-point kinetic energy arising through the Heisenberg uncertainty principle.

DOI: 10.1103/PhysRevE.100.062111

I. INTRODUCTION

Molecular dynamics simulation is the only direct way to determine the complete time dependence of the velocity autocorrelation function (VAF) of fluids. Together with other single-particle and collective properties, like the self- and total intermediate scattering functions, the VAF is a central quantity for understanding the microscopic processes and relaxation mechanisms that determine the overall dynamic behavior of liquids [1–3]. Pioneering simulation studies of the VAF and of the particle velocity field allowed researchers, for instance, to prove the existence of microscopic vortices in fluids [4] and to find an explanation for the so-called long-time tail (LTT) of the VAF, i.e., its slowly decaying behavior at long times that has been one of the principal and continuous motivations for studying this function [5–11].

More recently, significant progress in describing and interpreting the complete time dependence of the VAF has been made by exploiting the exponential series representation of time correlation functions [12–14]. For instance, the exponential mode decomposition of the VAF of a Lennard-Jones (LJ) fluid provided valuable information on the various dynamical processes determining the time behavior of the function on varying density and temperature [15,16]. Moreover, the exponential expansion was also shown to be very effective in representing other correlation functions of classical fluids [17]. Such results therefore suggested the extension of the methodology also to the case of quantum liquids, taking advantage of the fact that the exponential decomposition is readily applicable [14] to the Kubo transform of the velocity autocorrelation function (KVAF) [18]. In a very recent paper [19] we presented a subset of ring polymer molecular dynamics (RPMD) [20–23] simulations of the KVAF that we performed for dense fluid para-hydrogen (p-H_2). In particular, in Ref. [19] a study with varying temperature revealed very clearly the efficacy of the exponential mode decomposition of the KVAF at all the investigated temperatures. In this way, in full analogy with the classical case, the exponential modes of the KVAF could be associated with physical phenomena such as shear and longitudinal sound waves, diffusive processes, and vortices (LTT). Specifically, this allowed us to determine how the various microscopic mechanisms contribute individually to the translational mean kinetic energy (KE) per molecule $\langle K \rangle$ and, particularly, to a fundamental property such as its zero-point part $\langle K \rangle_0$.

Given the virtual impossibility to access the VAF of fluids experimentally, and the notorious difficulties in simulating the van Hove intermediate scattering functions directly in the quantum case, the simulated KVAF represents practically the only way to obtain information on the microscopic, collective, and single-particle, dynamical properties of a quantum liquid. In fact, it is well established that the motions of individual particles reflect all the dynamical processes, even those that are of collective nature. These unavoidably find a projection onto the KVAF, whose frequency spectrum is, as shown long ago by Rahman *et al.* [24], proportional to the density of states (DoS) of the quantum fluid, in the same way as the (classical) VAF spectrum is proportional to the DoS of a classical fluid [16,17]. In particular, because the collective excitations of longitudinal and transverse pseudophonons have been shown to determine the DoS shape at frequencies around the maxima of their respective dispersion curves, $\tilde{Z}(\omega)$ bears the signature of such molecular motions, and their presence can be linked to specific modes in the exponential expansion of the KVAF.

Here we thus exploit the exponential mode decomposition not only to relate the various features of the DoS to specific

*Corresponding author: guarini@fi.infn.it

collective and single-particle properties, as done in our previous works on classical fluids, but we also investigate the role of density on each mode in the case of a quantum fluid, where the particles' confinement in the cage of their neighbors plays a very important role.

In addition, we will exploit the direct relation existing between the mode expansion of the KVAF and the $t = 0$ value of the standard quantum mechanical VAF $u(t)$. In particular, the mean translational kinetic energy determined by $u(0) = 2\langle K\rangle/M$ (with M the molecular mass) was recently shown to have an explicit representation in terms of the modes of the KVAF [19]. An analogous representation was found to hold for the zero-point part $\langle K\rangle_0$ of the KE, providing the remarkable opportunity to understand the dynamical origin of this fundamental quantum property due to the Heisenberg uncertainty principle and accounting for the large value of the KE per particle [19,25–27], which, except at very high temperatures or very low densities, differs considerably from the classical value $3/(2\beta)$, where $\beta = 1/(k_B T)$ (k_B being the Boltzmann constant).

In this work, we focus on the density behavior of p-H_2 at a slightly supercritical temperature $T = 35$ K ($T_{cr} = 32.94$ K [28]). For this purpose we performed RPMD simulations of the KVAF, with $N = 864$ polymers interacting through the Silvera-Goldman potential [29], at six number densities ranging from the critical one ($n_{cr} = 9.37$ nm^{-3} [28]) to densities close to the melting curve ($\simeq$27% higher than the triple point density $n_{tr} = 23.01$ nm^{-3} [28]). The calculations were carried out in exactly the same way as reported in Refs. [19,27], to which we direct the reader for the computational details.

Similarly to the case of a LJ fluid [15,16], the results of our analysis will show that the evolution of the fitted exponential terms, as far as their number, nature, intensity, and timescale are concerned, permit the identification of some of the modes with specific dynamical properties. In particular, the already recognized role of slowly decaying exponentials in accounting for the LTT [15,16,19] is further confirmed here for p-H_2. In comparison with the LJ study, we also find a similar density evolution of the other modes, indicating the presence of longitudinal acoustic waves and the onset, at the higher densities, of a transverse collective dynamics.

II. THEORETICAL FRAMEWORK AND REFERENCE FORMULAS

The complex-valued standard quantum VAF of an N-particle system is

$$u(t) = \frac{1}{N}\sum_{\alpha=1}^{N}\langle \hat{\mathbf{v}}_\alpha(0)\cdot\hat{\mathbf{v}}_\alpha(t)\rangle, \tag{1}$$

where $\hat{\mathbf{v}}_\alpha(t)$ is the velocity operator of the αth molecule at time t, and the angular brackets denote a quantum statistical average. The frequency spectrum of $u(t)$, $p(\omega) = \frac{1}{2\pi}\int_{-\infty}^{\infty} dt\,\exp(-i\omega t)\,u(t)$, obeys the detailed balance principle

$$p(\omega) = e^{\beta\hbar\omega}p(-\omega), \tag{2}$$

where $\hbar = h/(2\pi)$ is the reduced Planck constant. Its symmetric and antisymmetric parts, $p_S(\omega)$ and $p_A(\omega)$, are related to the frequency spectrum $\tilde{Z}(\omega)$ of the KVAF $Z(t)$ by [18,24]

$$\tilde{Z}(\omega) = \frac{\tanh(\beta\hbar\omega/2)}{\beta\hbar\omega/2}\,p_S(\omega) = \frac{1}{\beta\hbar\omega/2}\,p_A(\omega). \tag{3}$$

Equivalently, a relation exists, via the Bose factor, between $p(\omega)$ and $\tilde{Z}(\omega)$:

$$p(\omega) = \frac{\beta\hbar\omega}{1-e^{-\beta\hbar\omega}}\tilde{Z}(\omega). \tag{4}$$

In contrast to $u(t)$, $Z(t)$ is an even and real-valued function in the time domain and at $t = 0$ provides the classical value $Z(0) = \langle \mathbf{v}^2\rangle = 3/(M\beta)$. The spectrum $\tilde{Z}(\omega)$ is also real and symmetric, while, as expressed by Eq. (2), $p(\omega)$ is a nonsymmetric function of frequency, with nonvanishing odd frequency moments.

The value of the quantum VAF at time zero, $u(0)$, can be calculated directly as the zeroth frequency moment of $p(\omega)$, i.e., as

$$u(0) = \int_{-\infty}^{\infty} d\omega\, p(\omega) = 2\int_0^{\infty} d\omega\, p_S(\omega). \tag{5}$$

Therefore, using the first of Eqs. (3), an RPMD estimate of $Z(t)$ provides one of the possible ways to determine the mean KE per molecule [30]:

$$\langle K\rangle = \frac{3}{2Z(0)}\int_0^{\infty} d\omega\,\frac{\hbar\omega}{\tanh(\beta\hbar\omega/2)}\tilde{Z}(\omega). \tag{6}$$

In analogy with a solid-state treatment, one can separate $\langle K\rangle_0$, that is, the zero-point part of the KE, from the thermally activated one [19,31]. The latter, given by the difference $\langle K\rangle - \langle K\rangle_0$, is the fraction of $\langle K\rangle$ due to the nonzero occupancy of the excited states of the system at $T > 0$. The zero-point part can be calculated directly from the simulations using, for instance, the zero-temperature version of Eq. (6), which is [32]

$$\langle K\rangle_0 = \frac{3}{2Z(0)}\int_0^{\infty} d\omega\,\hbar\omega\tilde{Z}(\omega). \tag{7}$$

In Ref. [19], which focused on the behavior with temperature along a single isochore, we found that the large value of $\langle K\rangle$, at a rather high p-H_2 density, is predominantly due to the zero-point component $\langle K\rangle_0$. At the even higher densities considered in the present study, we expect both $\langle K\rangle_0$ and $\langle K\rangle$ to increase further because a decrease of the volume available per particle implies, according to the Heisenberg uncertainty principle, a corresponding increase of the particle momentum.

In the following we will write the mode decomposition of both $\langle K\rangle_0$ and $\langle K\rangle$ in terms of the exponential modes of the *normalized* autocorrelation function $Z_n(t)$, which is

$$Z_n(t) = Z(t)/Z(0) = \sum_{j=1}^{\infty} I_j \exp(z_j|t|). \tag{8}$$

Being by construction an even function of time, $Z_n(t)$ as defined by Eq. (8) is thus expressed as an infinite sum of exponentials characterized, in general, by a complex amplitude I_j and a complex frequency z_j. Pure exponential decays of $Z_n(t)$ are accounted for in the series by what we will refer to as "real modes," i.e., having both I_j and z_j real, with $z_j < 0$. Damped oscillatory modes of $Z_n(t)$ are represented in the

series by what we will designate as "complex pairs," i.e., by $I_j \exp(z_j|t|) + I_j^* \exp(z_j^*|t|)$, with both I_j and z_j complex, and $\mathrm{Re}[z_j] < 0$.

Given the representation of Eq. (8), the frequency spectrum of the normalized KVAF now reads

$$\frac{\tilde{Z}(\omega)}{Z(t=0)} = \sum_{j=1}^{\infty} L_j(\omega) = \sum_{j=1}^{\infty} \frac{1}{\pi} \mathrm{Re}\left[\frac{I_j}{i\omega - z_j}\right], \tag{9}$$

where $L_j(\omega)$ is a "generalized" Lorentzian line. If I_j and z_j are real, then $L_j(\omega)$ is a genuine Lorentzian centered at $\omega = 0$. If I_j and z_j are complex, then the corresponding mode and its complex conjugate add up to give a pair of distorted Lorentzians centered at the nonzero frequencies $\pm\mathrm{Im}\,[z_j]$ [see Eq. (4) of Ref. [17] for details]. Finally, it is useful to recall that the continuity of a time autocorrelation function and the existence of its kth order ($k = 0, 1, 2, \ldots$) time derivatives at $t = 0$ lead, in the exponential representation of $Z_{\mathrm{n}}(t)$, to an infinite set of sum rules of the form

$$\sum_{j=1}^{\infty} I_j z_j^k = \left.\frac{d^k Z_{\mathrm{n}}(t)}{dt^k}\right|_{t=0}. \tag{10}$$

In particular, the zeroth ($\sum_{j=1}^{\infty} I_j = 1$) and first ($\sum_{j=1}^{\infty} I_j z_j = 0$) sum rules express the normalization and the vanishing of $\dot{Z}_{\mathrm{n}}(t)$ at $t = 0$, respectively.

Mode decomposition of the kinetic energy

In order to find the mode decomposition of the KE, we perform the frequency integration indicated in Eq. (6) via the convolution theorem, i.e., by replacing the integral of the product of functions over frequency space with the $t = 0$ value of the convolution of their inverse Fourier transforms. This can readily be done by exploiting the mathematically well-behaved kernel that Braams and co-workers [33] derived to obtain the quantum $u(t)$ from the knowledge of $Z(t)$. In particular, these authors showed that $\mathrm{Re}[u(t)]$ can be expressed as

$$\mathrm{Re}[u(t)] = Z(t) + \int_{-\infty}^{\infty} dt' k_1(t - t')\ddot{Z}(t') \tag{11}$$

with the kernel k_1 given by

$$k_1(t) = \frac{\beta\hbar}{2\pi} \log\left(1 - e^{-\frac{2\pi}{\beta\hbar}|t|}\right). \tag{12}$$

Here we are concerned with the $t = 0$ value of Eq. (11), which, given the even character of both $k_1(t)$ and $\ddot{Z}(t)$, can be written as

$$u(0) = Z(0) + 2\int_0^{\infty} dt\, k_1(t)\ddot{Z}(t). \tag{13}$$

Inserting the exponential representation for $Z_{\mathrm{n}}(t)$ [Eq. (8)], we obtain

$$u(0) = Z(0)\left[1 + \frac{\beta\hbar}{\pi}\int_0^{\infty} dt\, \log\left(1 - e^{-\frac{2\pi}{\beta\hbar}t}\right) \sum_{j=1}^{\infty} I_j z_j^2 \exp(z_j t)\right], \tag{14}$$

which casts into an explicit form the contribution of each mode to $u(0)$. By defining a new variable $y = e^{-\frac{2\pi}{\beta\hbar}t}$ it is possible to express $u(0)$ as

$$u(0) = Z(0)\left[1 + 2\left(\frac{\beta\hbar}{2\pi}\right)\sum_{j=1}^{2\infty} I_j z_j^2 \int_0^1 dy \log(1 - y)\, y^{-\frac{\beta\hbar}{2\pi}z_j - 1}\right], \tag{15}$$

with $\mathrm{Re}[-\frac{\beta\hbar}{2\pi}z_j] > 0$, and finally (see 4.293.8 in Ref. [34]) as

$$u(0) = Z(0)\left\{1 + \frac{\beta\hbar}{\pi}\sum_{j=1}^{\infty} I_j z_j \left[\psi\left(1 - \frac{\beta\hbar}{2\pi}z_j\right) + \gamma\right]\right\}, \tag{16}$$

where ψ is the digamma function and γ is the Euler-Mascheroni constant. By also replacing $Z(0)$ by $3/(m\beta)\sum_{j=1}^{\infty} I_j$, one finally finds for the mean KE

$$\langle K\rangle = \frac{3\hbar}{2\pi}\sum_{j=1}^{\infty} I_j \left\{\frac{\pi}{\beta\hbar} + z_j\left[\psi\left(1 - \frac{\beta\hbar}{2\pi}z_j\right) + \gamma\right]\right\}. \tag{17}$$

In order to write an analogous representation for the zero-point contribution, $\langle K\rangle_0$, to the kinetic energy, one can either repeat the above derivation starting from Eq. (7) instead of Eq. (6) or equivalently exploit the asymptotic behavior of Eq. (17). By retaining the leading term in the asymptotic series for the digamma function at large values of its argument [see (6.3.18) in Ref. [35]], we obtain

$$\langle K\rangle_0 = \frac{3\hbar}{2\pi}\sum_{j=1}^{\infty} I_j z_j \left[\log\left(-\frac{\beta\hbar}{2\pi}z_j\right) + \gamma\right], \tag{18}$$

which will be discussed later in the paper. Here it is important to stress that $\langle K\rangle_0$ and $\langle K\rangle$ have no relation with the classical value of the KE, except in the limit of high temperature or low density. Therefore, $\langle K\rangle_0$ should not be interpreted as the deviation of $\langle K\rangle$ from $3/(2\beta)$.

III. MULTIEXPONENTIAL ANALYSIS OF THE SIMULATED KVAF

Practical applications of the mode decomposition of course require a truncation of the infinite series of Eq. (8). We showed in our previous studies that a small number of real and complex terms is typically sufficient to provide an extremely good representation of the correlation functions considered so far [15–17,19]. As in our earlier investigations, we have also here employed a number of constraints, when fitting these modes (i.e., the respective I_j and z_j) to the simulated KVAFs, in order to incorporate the normalization condition, $\sum_j I_j = 1$, and to enforce the first few odd sum rules dictated by Eq. (10) up to $k - 1$, where k is even. Given the specific form our finite mode expansion, which is infinitely often differentiable except at $t = 0$, this not only ensures that the odd derivatives of $Z(t)$ up to order $k - 1$ vanish at $t = 0$, but that all derivatives up to order k exist and are finite at the origin.

The analysis of the time dependence of the KVAF is thus performed by fitting the sum of a finite number of exponential terms to the data, with I_j and z_j as parameters. The total number of terms in the series, the number of real and complex ones, and the set of sum rules to be imposed is essentially dictated by physical considerations and, eventually, by the fit quality achieved with a reasonably low (ideally

TABLE I. Temperature T and number density n of the thermodynamic states of p-H_2 considered for the simulations. The critical (subscript cr) and triple (subscript tr) point density and temperature are from Ref. [28]. The average collision time t_0 is also reported for each state (see Sec. IV). The zero-point and total translational kinetic energy calculated via Eqs. (7) and (6), respectively, are expressed in units of K and are also plotted in Fig. 4. p-H_2 ($T = 35$ K); $n_{cr} = 9.37$ nm^{-3}, $T_{cr} = 32.94$ K; $n_{tr} = 23.01$ nm^{-3}, $T_{tr} = 13.80$ K.

n [nm^{-3}]	t_0 [ps]	$\langle K\rangle_0/k_B$ [K]	$\langle K\rangle/k_B$ [K]
10.61	0.115	31.89	64.17
14.33	0.098	40.15	68.52
18.05	0.084	49.88	74.03
21.77	0.071	62.08	81.96
25.49	0.060	76.88	92.49
29.21	0.051	94.09	105.9

minimized) number of parameters. Moreover, in regions of thermodynamic phase diagram where a dynamical crossover may be expected to occur (cf. Table III of Ref. [16] for the LJ fluid), the model must be chosen flexible enough to account for physical changes induced in the microscopic dynamics by an increase of density. For instance, in our previous experience, we found that a small number of real modes is required in high-density states around and above the triple point density. At our supercritical temperature, one of these always represents the LTT mentioned in the Introduction. Longitudinal sound waves must also be accounted for by a complex pair at all densities, while shear waves are detectable in the dynamical properties only in high-density states. In fact, the clear need to introduce a low-frequency complex pair in the fit model in order to obtain an accurate description of the KVAF may be taken to be the hallmark of the dynamical change associated with the ability of the (denser) fluid to also sustain transverse oscillations, which are absent at lower densities.

According to the above schematization, first applied in the LJ case from low to high density [16], and subsequently confirmed in the high-density temperature study of Ref. [19], we adopt a similar procedure for the present density study of p-H_2 at constant temperature, as detailed below. For reference, the thermodynamical conditions of the RPMD simulations are summarized in Table I. To put them in perspective, we also included the fixed (critical and triple) points of the phase diagram of p-H_2 [28].

Specifically, for the three *low-density states* of p-H_2, we obtained very good fits to $Z_n(t)$ by considering three real modes and two complex pairs, and imposing *four* sum rules. The latter correspond, of course, to the zeroth frequency moment (normalization) $\sum_j I_j = 1$ and the conditions $\sum_j I_j z_j^{k-1} = 0$ for $k = 2, 4, 6$, ensuring the vanishing of all odd derivatives at $t = 0$ up to fifth order.

In the following, a labeling of the modes consistent with that adopted in Refs. [16,19] will be used. Therefore, the three real modes mentioned above will be referred to as R2, R3, and R4, and the two complex pairs will be indicated by C1 and C2, with the same physical interpretation as for the LJ system. In particular, R4 corresponds to the slowest decaying real mode (LTT). We recall that, while C2 in our nomenclature is related to the contribution of longitudinal waves, C1 is a very high-frequency, strongly damped mode of nearly negligible intensity whose origin is still unclear, but which seems to be essential for a good description of the low-density KVAF at very short times. Interestingly, in the present case of p-H_2, C1 ceases to be necessary in complex form as soon as a genuine transverse dynamics sets in, i.e., in the high-density case discussed below.

Concerning the three *high-density states*, an excellent description of the KVAF and its spectrum was obtained by considering two real modes and two complex pairs, satisfying *three* sum rules. In this case, the decay channels of $Z(t)$ will be referred to as R1 and R4 (real modes) and C2, C3 (complex pairs). This labeling scheme was chosen in order to indicate in a natural way that the slowest decaying mode (R4) is actually present at *all* densities, as we will show below. The same holds for the damped longitudinal oscillatory component (C2). By contrast, the new real mode (R1) at high density seems to originate from a vanishing of the oscillatory part of the C1 pair found at low density. It is important to stress that, exactly as in the LJ case, the increase of density leads to the disappearance of the faster real modes mentioned before (R2 and R3), and the emergence of a complex pair C3 at high density, as reflected by the labeling scheme. Also, in high-density p-H_2, C3 can be recognized to be the fingerprint, in the density of states $\tilde{Z}(\omega)$ (and therefore in the KVAF), of the existence of low-frequency transverse propagating waves in the medium, with a typically very weak dispersive character that is responsible for the main maximum in the DoS [16,17].

Thus, a remarkable consistency is found in the *kind* of processes that, according to the exponential decomposition, account for the entire time behavior of the VAF, irrespective of quantum delocalization effects. In fact, the density dictates, in more or less the same way, the emergence or disappearance of real and complex modes in the VAF both in a classical LJ system and in a moderate quantum fluid like p-H_2. One of the outcomes of the present work regards the better identification of the evolution that C1 (at low densities) undergoes after a clear, density-driven transition in the dynamics: the complex high-frequency mode at low density becoming, apparently, a very fast real decay (R1) at high density.

The fit results for one low- and one high-density state at 35 K are reported in Fig. 1. The various fit components are also plotted separately and identified in the legend, both for the KVAF and for the spectra. The latter are shown using a semilogarithmic scale in order to appreciate the very good performance of the model over nearly three decades. In Figs. 1(c) and 1(d) the tiny peak at $\omega = 0$ hints at the presence of an LTT at both states. The onset of shear modes (low-frequency shoulders evolving into maxima of the DoS with increasing density) is also evident.

IV. DENSITY BEHAVIOR AND MODE CONTRIBUTIONS TO DIFFUSION

Figure 2 shows the density dependence of the damping, $-z_j$, of the various real modes [Fig. 2(a)], and the damping, $-\mathrm{Re}[z_j]$ [Fig. 2(b)], and frequency, $\mathrm{Im}[z_j]$ [Fig. 2(c)], of the oscillatory modes related to wave propagation in the fluid. The trends look rather smooth, indicating that the fit at a

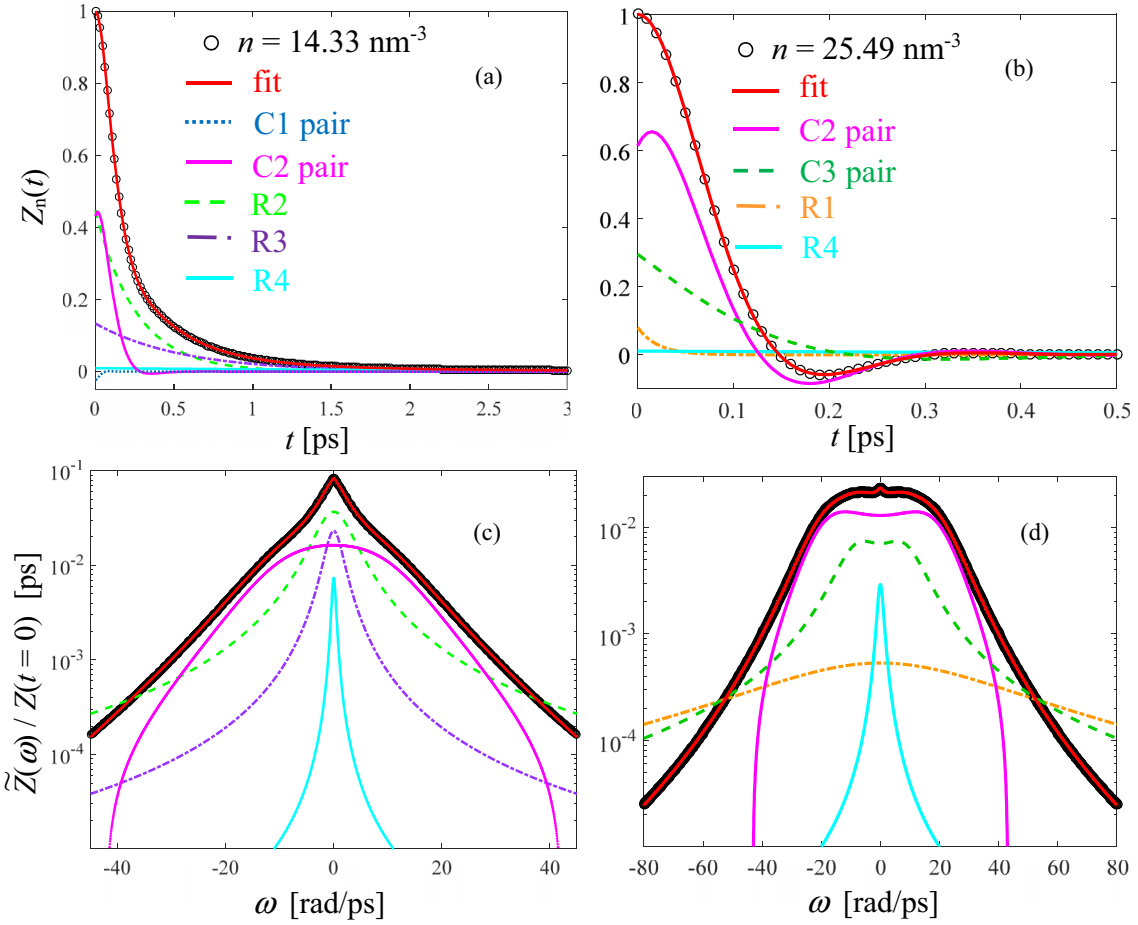

FIG. 1. Fit results for one low-density (left panels) and one high-density (right panels) state of p-H_2 at $T = 35$ K. The normalized KVAFs are shown in the upper panels (a) and (b). Lower panels (c) and (d) report the corresponding spectra on a semilogarithmic scale. The various fit components are shown separately, as specified in the legend. Their sum provides the fit curve (red solid line) which is in perfect agreement with the simulation data (black empty circles).

given density is consistent with the one at the successive density and so on. Also, there is consistency in the density dependence of the modes (R4 and C2) present across the mentioned dynamical transition. A drastic change is observed only in the imaginary part of C3, which is very low at the first density at which such a mode is required to obtain a good fit, probably indicating that, although the fit is sensitive to its presence, C3 lacks a fully propagating character. Conversely, the longitudinal component C2 varies smoothly with density and becomes less damped in approaching the triple point density, while its frequency grows monotonically, as expected.

Similar to our analysis of the LJ fluid [15,16], it is interesting to estimate the average number of collisions involved in the loss of velocity correlation brought about by the various processes, and to understand if there are differences between p-H_2 and a classical fluid. In the quantum case, an appropriate characteristic timescale must be chosen to replace the classical Enskog mean free time between collisions of hard spheres [15,16], which the presence of delocalization effects renders too drastic an approximation. As demonstrated in Ref. [27], a more appropriate time scale is the average collision time t_0, i.e., the inverse of the Einstein frequency Ω_0 [3]. The latter can be determined either by fits of the short time behavior of the normalized KVAF or directly from the multiexponential analysis, since $\Omega_0^2 = -\sum_j I_j z_j^2$. Both methods provided the t_0 values reported in Table I. Denoting by $\tau_j = -1/\mathrm{Re}[z_j]$ the decay times of the various modes, we show the scaled quantities τ_j/t_0 in Fig. 3.

The oscillatory modes C1 and C2 have the shortest decay times at low density. These correspond, on average, to less than or about one collision time and can thus be identified with the so-called binary processes contributing to the VAF behavior at short times [3]. Figure 3 also shows that the low-density real modes R2 and R3 correspond to about two to five collision times, implying that these modes require interactions among groups of a few particles before decaying, similar to the LJ fluid. By contrast, R4 involves some tens of collisions, nearly a factor five more than R3. This suggests that R4 originates from cooperative multiparticle motions, so it is this mode that likely reflects the "nonbinary" processes [3], leading to the slow loss of correlation of the VAF and to the manifestation of the LTT. However, quite differently from the LJ case, where the decay of R4 was found to span more than 60 collision times, here the number of collisions pertaining to R4 is considerably reduced to about 25. A possible reason for this difference might lie in the interaction properties. In fact, by performing an exponential mode decomposition of the Silvera-Goldman-based VAF of *classical* p-H_2, in the

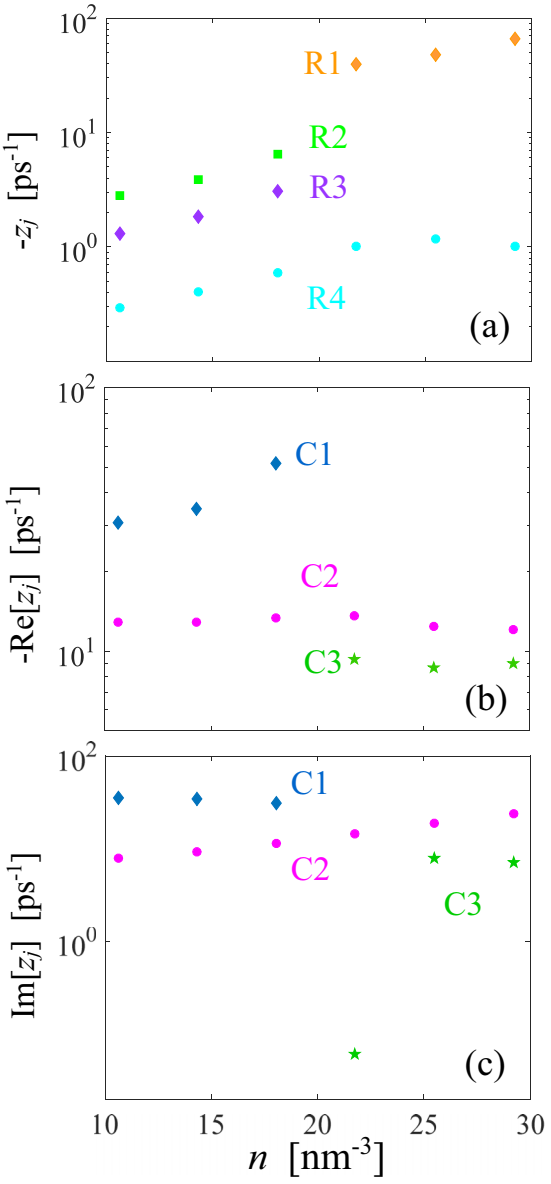

FIG. 2. Density dependence of the damping of real modes (a) and of the damping (b) and frequency (c) of the complex pairs associated with longitudinal and transverse waves.

thermodynamic " corresponding" states of Ref. [27], we found a LTT (R4) and a number of collisions involved in its decay again of the order of about 25. So, quantum effects are likely to be excluded in the explanation of the mentioned difference. These findings suggest a future useful comparison between quantum RPMD or CMD simulations of the KVAF based on either the LJ or the Silvera-Goldman potential.

We finally note that the agreement between the number of collisions involved in C1, at low density, and in R1, at high density, suggests that these two modes are in fact closely linked, and that the dynamical transition changes the complex character of C1, at low densities, into a real, fast decaying, mode (R1) at high densities.

It is also interesting to break down into contributions from real and complex modes the integral of the VAF, which is proportional to the self-diffusion coefficient D through a

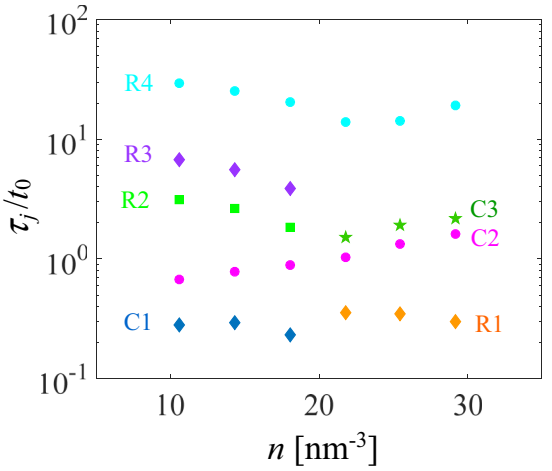

FIG. 3. Decay times τ_j of the fitted exponentials, in units of the collision time t_0, as functions of density. The various modes are identified as described in the text. The plotted quantities provide the average number of collisions involved in each decay mechanism.

well-known classical Green-Kubo relation [3], which can be easily shown to also hold for the quantum KVAF, owing to the spectral identity $\tilde{Z}(\omega = 0) = p_S(\omega = 0) = 3D/\pi$.

Table II shows the percentage contribution of individual modes (or groups of modes) to D, when pure decays are gathered together and compared to the significant oscillatory modes, at low (upper part of Table II) and high density (lower part of Table II). At low density, given the negligible intensity of the C1 mode, Table II reports its sum with C2, whereas, at high density, we give the C2 and C3 percentages separately, in order to show how transverse and longitudinal components share the largest contribution to D. Here no special difference is found between the classical LJ and the quantum p-H_2 case. At low density real modes are the main constituents of D, while at high density complex modes (damped propagating waves) become dominant in establishing the diffusion mechanism and, thereby, its macroscopic coefficient D.

V. MODE CONTRIBUTIONS TO $\langle K \rangle_0$ AND $\langle K \rangle$

Using the amplitudes and frequencies obtained from the fits, we are finally able to determine how the various

TABLE II. Percentage contribution, as a function of density, to the integral of the VAF of the purely decaying modes (grouped together) and of the damped oscillatory modes (grouped only at low density, as explained in the text). Upper rows report the low-density results; lower rows refer to the high-density states. p-H_2 ($T = 35$ K).

n [nm^{-3}]	10.61	14.33	18.05
R2+R3+R4	89.7	80.4	66.5
C1+C2	10.3	19.6	33.5
n [nm^{-3}]	21.77	25.49	29.21
R1+R4	21.0	13.7	3.0
C2	55.0	55.9	64.0
C3	24.0	30.4	33.0

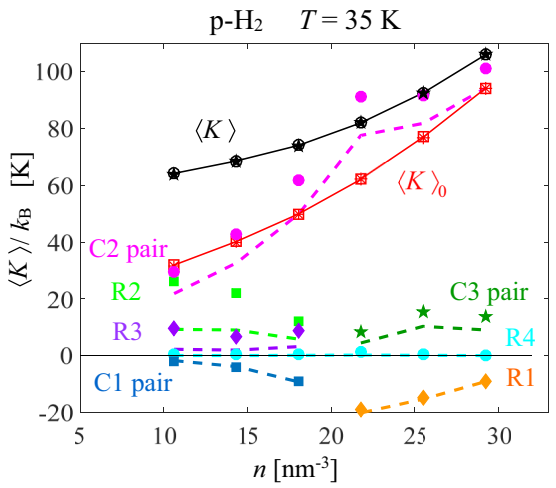

FIG. 4. Density dependence of the quantum translational kinetic energy, in units of K, as obtained by resummation of the individual modes of Eq. (17) (black full stars) or from the direct calculation of Eq. (6) (black open circles joined by the black solid line). Single terms of Eq. (17) are shown as: R1 (orange full diamonds), R2 (bright green squares), R3 (violet diamonds), R4 (cyan full circles), C1 (blue full squares), C2 (pink full circles), and C3 (green full stars). The individual zero-point contributions of Eq. (18) are displayed in the same color, but with dashed curves. That the symbols for the real modes R1 and R4 and the complex pair C1 fall onto the dashed curves indicates that they contribute only to the zero-point energy. The open red squares connected by solid line correspond to the direct calculation of $\langle K\rangle_0$ from Eq. (7). The resummation of the dashed curves, according to the expansion of Eq. (18), is displayed with red asterisks.

dynamical processes contribute to the translational kinetic energy by studying the individual terms of the series in Eqs. (17) and (18). Figure 4 shows the density behavior of each real mode and each complex pair: Dashed curves are the contributions to the zero-point KE, while full symbols include the effect of temperature and represent the contributions to the total KE. A resummation of the dashed curves perfectly coincides with the $\langle K\rangle_0$ value obtained from the direct calculation of Eq. (7) shown as a red curve through empty squares. Similarly, the sum of the full symbols agrees very well with the values computed from Eq. (6) and displayed as a black line joining empty circles. Numerical values of $\langle K\rangle_0$ and $\langle K\rangle$ can be found in Table I. As expected, the zero-point energy grows with density because the more restrictive confinement of particles translates, quantum mechanically, into an increase of their momentum. It is seen, however, that, although we are moving along an isotherm, the total KE grows less rapidly than $\langle K\rangle_0$, meaning that the thermally activated part of the KE decreases with increasing density. This can be understood by analogy with the case of a solid, where an increase of density corresponds to a narrower potential well with higher energy levels, so that the occupation probability of excited states diminishes.

In addition to these general considerations, the high-density part of Fig. 4 confirms the results of Ref. [19] and the dominant role of longitudinal waves (C2) in determining the KE, with their larger and larger contribution to both $\langle K\rangle_0$ and $\langle K\rangle$ as confinement grows. The contribution of the LTT is minute, given the very different, nonbinary, dynamical origin of R4, which represents an extremely slow multiparticle process of almost negligible intensity [19]. Moreover, it is seen that the KE, at all densities, results from a cancellation of effects, given the negative contributions of either the C1 pair (at low density) or R1 (at high density). From a mathematical point of view, these are dictated by the extremely large damping of the modes, which implies, e.g., for a real mode with positive amplitude like R1, that $-\beta\hbar z_j/(2\pi)$ takes a large and positive value. Therefore, $z_j \log[-\beta\hbar z_j/(2\pi)]$ in Eq. (18) is negative for R1. A similar consideration holds for the C1 pair, although the mathematics of complex modes is less transparent and difficult to detail. That the contributions of R1 and C1 are negative can be ascribed to a diffusive-like fast decaying character of these modes (even when they are complex), which works in opposition to the particles' local confinement. This can be realized by noting that the density and temperature behavior of the R1 component in the KE is consistent with a diffusion process. In fact, R1 was found to become more negative as T is raised [19], while here it is seen to increase slightly (become less negative) with n. Both trends imply that the more diffusion increases with T (decreases with n), the more (the less) the confinement will be counteracted by R1. The reason why, at low density, C1 does not display the same diffusive-like trend as R1 is probably due to the interplay between the real and imaginary parts of amplitude and frequency of this mode, which transforms into a genuine diffusion process (with the expected density dependence) only above the triple point density, i.e., after the dynamical crossover.

In Fig. 4 the coincidence of dashed curves and symbols for these modes indicates that they affect mainly the zero-point energy, without any relevant influence on the thermally activated part of $\langle K\rangle$. Indeed, it is not evident why R1 and C1 contribute only to $\langle K\rangle_0$. We can only state again that this common behavior of C1 and R1 suggests that they are probably different manifestations of the same dynamical process, which still escapes a full characterization, especially below the triple point density.

The low-density part of Fig. 4 provides further insight on the dynamical evolution of the system in general. Real modes at low density (R2 and R3) are seen to contribute significantly to both $\langle K\rangle_0$ and $\langle K\rangle$. For instance, the thermally activated part due to R2 is even larger than that of C2 in the neighborhood of the critical point. Moreover, the comparison of the behavior of R3 (at low density) and C3 (at high density) seems to indicate an analogous, though reversed, relationship with respect to the one between C1 and R1: In this case, a real mode at low density seems to evolve into a complex pair, with a nonvanishing characteristic frequency, at high density. In other words, R3 (or R2 plus R3) might perhaps be interpreted as the low-density ancestors of the final transverse low-frequency mode C3.

VI. CONCLUSIONS

The present investigation extends and complements our previous work [19] on the dynamical interpretation of the VAF of p-H_2 by providing results of RPMD simulations

for a number of thermodynamic states along a supercritical isotherm, which were analyzed by means of an exponential mode representation. A general outcome of the whole work is that the semiquantum nature of fluid p-H_2 does not alter some general aspects of the dynamics of fluids. Like in classical systems, a certain scheme and meaning of the modes holds also in the quantum case. In particular, we found clear evidence of the existence of a dynamical modification in passing from close-to-critical to close-to-solidification density states. This is quite evidently in relation to the increased viscosity and shear stress resistance acquired by the fluid with growing density, and leading to propagating, though strongly damped, transverse excitations in the fluid.

As far as the mean KE is concerned, the present results fully corroborate the conclusions of our previous temperature study [19], namely, that (1) the origin of the large zero-point (and then total) KE values of a molecule in a quantum fluid and their growth with increasing density are a manifestation of the Heisenberg uncertainty principle, and (2) the contribution of longitudinal modes C2, which is comparable to that of R2 at low density, grows rapidly with density and becomes dominant at high density, as happened at all temperatures investigated at the high-density state of Ref. [19]. Concerning point (1), we observe that the effect can be interpreted as a consequence of the mutual confinement exerted by the fluid particles, due to the reduction of the effective volume available per molecule, enhanced by the increase of the excluded volume fraction in a dense fluid. On the other hand, as shown by Eq. (7), $\langle K\rangle_0$ is, to within a constant factor, the average excitation frequency in the KVAF spectrum, so that intense mode pairs with the highest frequency, i.e., C2, contribute most to the average. Thus, the smooth monotonic increase of the C2 oscillation frequency [see Fig. 2(c)] explains point (2). Of course, any effect of the even higher frequency characterizing the C1 pair at low densities is completely hidden by the negligible amplitude of this component, giving practically no contribution to the probability density represented by $\tilde{Z}(\omega)$ in Eq. (7).

Explaining the large zero-point and total KE quantum values, and their density dependence, as a manifestation of the Heisenberg uncertainty principle can be interpreted as evidence for the influence of the local structure on quantum behavior. This fact is in line with simulation results obtained for structural properties [36] and the VAF [37].

As mentioned, at the three highest densities studied here, the dynamical picture changes somewhat abruptly, due to the onset of propagating transverse excitations (C3) that makes $\tilde{Z}(\omega)$ more intense at their respective frequencies. At the same time, $\tilde{Z}(\omega)$ diminishes at the C2 frequency in order to satisfy the normalization condition, and the C2 contribution to the average frequency value is reduced. The onset of C3 thus partly mitigates the dominant role played by longitudinal modes, as shown in Fig. 4.

Thus, it can also be appreciated that the dynamical change across the triple point density, requiring a rather drastic modification of the scheme of the modes, does not affect the global, perfectly smooth trends of both $\langle K\rangle_0$ and $\langle K\rangle$. This might be taken as an indication of the reliability of our description of the density behavior of the KVAF. In fact, despite the clear change in the dynamics, our low- and high-density representations account very well, without discontinuities, for a static property like the KE.

ACKNOWLEDGMENTS

This research was funded by Ente Cassa di Risparmio Firenze (Grant No. 2016-0866) and by Ministero dell'Istruzione dell'Università e della Ricerca Italiano (Grant No. PRIN2017-2017Z55KCW).

[1] J. P. Boon and S. Yip, *Molecular Hydrodynamics* (Dover, New York, 1980).
[2] J. P. Hansen and I. R. McDonald, *Theory of Simple Liquids* (Academic Press, London, 1986).
[3] U. Balucani and M. Zoppi, *Dynamics of the Liquid State* (Clarendon, Oxford, 1994).
[4] B. J. Alder and T. E. Wainwright, Decay of the velocity autocorrelation function, Phys. Rev. A **1**, 18 (1970).
[5] D. Levesque and W. T. Ashurst, Long-Time Behavior of the Velocity Autocorrelation Function for a Fluid of Soft Repulsive Particles, Phys. Rev. Lett. **33**, 277 (1974).
[6] A. McDonough, S. P. Russo, and I. K. Snook, Long-time behavior of the velocity autocorrelation function for moderately dense, soft-repulsive, and Lennard-Jones fluids, Phys. Rev. E **63**, 026109 (2001).
[7] R. F. A. Dib, F. Ould-Kaddour, and D. Levesque, Long-time behavior of the velocity autocorrelation function at low densities and near the critical point of simple fluids, Phys. Rev. E **74**, 011202 (2006).
[8] K. Meier, A. Laesecke, and S. Kabelac, Transport coefficients of the Lennard-Jones model fluid. I. Viscosity, J. Chem. Phys. **121**, 3671 (2004).
[9] K. Meier, A. Laesecke, and S. Kabelac, Transport coefficients of the Lennard-Jones model fluid. II Self-diffusion, J. Chem. Phys. **121**, 9526 (2004).
[10] S. R. Williams, G. Bryant, I. K. Snook, and W. van Megen, Velocity Autocorrelation Functions of Hard-Sphere Fluids: Long-Time Tails Upon Undercooling, Phys. Rev. Lett. **96**, 087801 (2006).
[11] R. E. Ryltsev and N. M. Chtchelkatchev, Hydrodynamic anomalies in supercritical fluid, J. Chem. Phys. **141**, 124509 (2014).
[12] F. Barocchi, U. Bafile, and M. Sampoli, Exact exponential function solution of the generalized Langevin equation for autocorrelation functions of many-body systems, Phys. Rev. E **85**, 022102 (2012).
[13] F. Barocchi and U. Bafile, Expansion in Lorentzian functions of spectra of quantum autocorrelations, Phys. Rev. E **87**, 062133 (2013).
[14] F. Barocchi, E. Guarini, and U. Bafile, Exponential series expansion for correlation functions of many-body systems, Phys. Rev. E **90**, 032106 (2014).
[15] S. Bellissima, M. Neumann, E. Guarini, U. Bafile, and F. Barocchi, Time dependence of the velocity autocorrelation

function of a fluid: An eigenmode analysis of dynamical processes, Phys. Rev. E **92**, 042166 (2015).

[16] S. Bellissima, M. Neumann, E. Guarini, U. Bafile, and F. Barocchi, Density of states and dynamical crossover in a dense fluid revealed by exponential mode analysis of the velocity autocorrelation function, Phys. Rev. E **95**, 012108 (2017).

[17] E. Guarini, S. Bellissima, U. Bafile, E. Farhi, A. De Francesco, F. Formisano, and F. Barocchi, Density of states from mode expansion of the self-dynamic structure factor of a liquid metal, Phys. Rev. E **95**, 012141 (2017).

[18] R. Kubo, The fluctuation-dissipation theorem, Rep. Prog. Phys. **29**, 255 (1966).

[19] E. Guarini, M. Neumann, U. Bafile, S. Bellissima, and D. Colognesi, Dynamical Origin of the Total and Zero-Point Kinetic Energy in a Quantum Fluid, Phys. Rev. Lett. **123**, 135301 (2019).

[20] I. R. Craig and D. E. Manolopoulos, Quantum statistics and classical mechanics: Real time correlation functions from ring polymer molecular dynamics, J. Chem. Phys. **121**, 3368 (2004).

[21] T. F. Miller III and D. E. Manolopoulos, Quantum diffusion in liquid para-hydrogen from ring-polymer molecular dynamics, J. Chem. Phys. **122**, 184503 (2005).

[22] I. R. Craig and D. E. Manolopoulos, Inelastic neutron scattering from liquid *para*-hydrogen by ring polymer molecular dynamics, Chem. Phys. **322**, 236 (2006).

[23] S. Habershon, D. E. Manolopoulos, T. E. Markland, and T. F. Miller III, Ring-polymer molecular dynamics: Quantum effects in chemical dynamics from classical trajectories in an extended phase space, Annu. Rev. Phys. Chem. **64**, 387 (2013).

[24] A. Rahman, K. S. Singwi, and A. Sjölander, Theory of slow neutron scattering by liquids. I, Phys. Rev. **126**, 986 (1962).

[25] M. Celli, D. Colognesi, and M. Zoppi, Direct experimental access to microscopic dynamics in liquid hydrogen, Phys. Rev. E **66**, 021202 (2002).

[26] D. Colognesi, M. Celli, M. Neumann, and M. Zoppi, Microscopic self-dynamics in liquid hydrogen and in its mixtures with deuterium, Phys. Rev. E **70**, 061202 (2004).

[27] S. Bellissima, M. Neumann, U. Bafile, D. Colognesi, F. Barocchi, and E. Guarini, Density and time scaling effects on the velocity autocorrelation function of quantum and classical dense fluid *para*-hydrogen, J. Chem. Phys. **150**, 074502 (2019).

[28] E. W. Lemmon, M. O. McLinden, and D. G. Friend, Thermophysical properties of fluid systems, in *NIST Chemistry WebBook*, NIST Standard Reference Database Number 69, edited by P. J. Linstrom and W. G. Mallard (National Institute of Standards and Technology, Gaithersburg, MD, 2017), http://webbook.nist.gov.

[29] I. F. Silvera and V. V. Goldman, The isotropic intermolecular potential for H_2 and D_2 in the solid and gas phases, J. Chem. Phys. **69**, 4209 (1978).

[30] The mean kinetic energy can alternatively be derived from the intrapolymer spring energies of either RPMD or path-integral Monte Carlo simulations. In general, these values are within 2%–3% of the results obtained with Eq. (6), as shown in Table IV of Ref. [27].

[31] M. Zoppi, D. Colognesi, and M. Celli, Density dependence of mean kinetic energy in liquid and solid hydrogen at 19.3 K, Eur. Phys. J. B **23**, 171 (2001).

[32] Note that in Eq. (7), $\tilde{Z}(\omega)$ is evaluated at the actual temperature of the fluid. The concept of zero-point mean kinetic energy is the natural extension to a quantum fluid of a key physical quantity which originally appears in the phonon dynamics of a solid crystal, because $\tilde{Z}(\omega)$ is the liquid-state counterpart of the density of phonon states $G(\omega)$ and shares with it the property of determining the single-particle mean kinetic energy $\langle K\rangle$ through Eq. (6) [see, e.g., K. S. Singwi and M. P. Tosi, Phys. Rev. **149**, 70 (1966)]. In the most trivial case, the so-called Einstein solid, $G(\omega) = \delta(\omega - \omega_0)$ and a single three-dimensional harmonic oscillator represents the full phonon dynamics of the system. Here one sees that $\langle K\rangle_0 = (3/4)\hbar\omega_0$, while $\langle K\rangle = (3/4)\hbar\omega_0 \coth(\beta\hbar\omega_0)$, in full agreement with Eqs. (6) and (7).

[33] B. J. Braams, T. F. Miller III, and D. E. Manolopoulos, Sum rule constraints on Kubo-transformed correlation functions, Chem. Phys. Lett. **418**, 179 (2006).

[34] I. S. Gradshteyn and I. M. Ryzhik, *Tables of Integrals, Series, and Products*, 7th ed. (Elsevier Academic Press, New York, 2007).

[35] M. Abramowitz and I. A. Stegun, *Handbook of Mathematical Functions, with Formulas, Graphs, and Mathematical Tables* (Dover, New York, 1964).

[36] R. Potestio and L. Delle Site, Quantum locality and equilibrium properties in low-temperature parahydrogen: A multiscale simulation study, J. Chem. Phys. **136**, 054101 (2012).

[37] A. Agarwal and L. Delle Site, Grand-canonical adaptive resolution centroid molecular dynamics: Implementation and application, Comput. Phys. Commun. **206**, 26 (2016).